The human cytomegalovirus protein UL147A downregulates the most prevalent MICA allele: MICA*008, to evade NK cell-mediated killing

Einat Seidel[a¶], Liat Dassa[a¶], Esther Oiknine-Djian[b,c,d], Dana G. Wolf[b,c,d], Vu Thuy Khanh Le-Trilling[e&*] and Ofer Mandelboim[a&*]

[a]The Lautenberg Center for General and Tumor Immunology, The Faculty of Medicine, The Hebrew University Medical School, IMRIC, Jerusalem, Israel

[b]Clinical Virology Unit, Hadassah Hebrew University Medical Center, Jerusalem, Israel

[c]Department of Biochemistry, IMRIC, Jerusalem, Israel

[d]The Chanock Center for Virology, IMRIC, Jerusalem, Israel

[e]Institute for Virology of the University Hospital Essen, University Duisburg-Essen, Essen, Germany

¶ E.S. and L.D. contributed equally to this article.

& V.T.K.L.-T and O.M. contributed equally to this article.

* Address correspondence to Khanh.Le@uk-essen.de (V.T.K.L.-T), or oferm@ekmd.huji.ac.il (O.M.).

Running title: UL147A downregulates MICA*008

Abstract

Natural killer (NK) cells are innate immune lymphocytes capable of killing target cells without prior sensitization. NK cell activity is regulated by signals received from activating and inhibitory receptors. One pivotal activating NK receptor is NKG2D, which binds a family of eight ligands, including the major histocompatibility complex (MHC) class I-related chain A (MICA). Human cytomegalovirus (HCMV) is a ubiquitous betaherpesvirus causing morbidity and mortality in immunosuppressed patients and congenitally infected infants. HCMV encodes multiple antagonists of NK cell activation, including many mechanisms targeting MICA. However, only one of these mechanisms counters the most prevalent MICA allele, MICA*008. Here, we discover that a hitherto uncharacterized HCMV protein, UL147A, specifically targets MICA*008 to proteasomal degradation, thus hindering the elimination of HCMV-infected cells by NK cells. Mechanistic analyses disclose that the non-canonical GPI anchoring pathway of immature MICA*008 constitutes the determinant of UL147A specificity for this MICA allele. These findings advance our understanding of the complex and rapidly evolving HCMV immune evasion mechanisms, which may facilitate the development of antiviral drugs and vaccines.

Author Summary

Human cytomegalovirus (HCMV) is a common pathogen that usually causes asymptomatic infection in the immunocompetent population, but the immunosuppressed and fetuses infected *in utero* suffer mortality and disability due to HCMV disease. Current HCMV treatments are limited and no vaccine has been approved, despite significant efforts. HCMV encodes many genes of unknown function, and virus-host interactions are only partially understood. Here, we discovered that a hitherto uncharacterized HCMV protein, UL147A, downregulates the expression of an activating immune ligand allele named MICA*008, thus hindering the elimination of HCMV-infected cells. Elucidating HCMV immune evasion mechanisms could aid in the development of novel HCMV treatments and vaccines. Furthermore, MICA*008 is a highly prevalent allele implicated in cancer immune evasion, autoimmunity and graft rejection. In this work we have shown that UL147A interferes with MICA*008's poorly understood, nonstandard maturation pathway. Study of UL147A may enable manipulation of its expression as a therapeutic measure against HCMV.

Introduction

Human cytomegalovirus (HCMV) is a betaherpesvirus with a large double stranded DNA genome of approximately 235 kilo base pair (kbp) (1). HCMV encodes 170 canonical genes and recent work has additionally described noncanonical open reading frames, as well as several classes of small and large noncoding RNAs (2–7). Of note, the functions of many of its genes remain unknown (8).

Infection with HCMV in healthy individuals is usually asymptomatic but results in lifetime persistence, due to HCMV's remarkable ability to evade host immune responses (9). In immunosuppressed individuals, HCMV causes significant morbidity with a wide range of end-organ involvement, indirect complications such as increased graft rejection in transplant recipients and mortality. HCMV is also a common congenitally transmitted pathogen, which can cause sensorineural hearing loss and developmental delays in children born infected with HCMV (1,10). The use of available drug treatments for HCMV is often limited by their significant toxicity (1), and though there are several promising candidates in development, no HCMV vaccine has been approved for use (11). As a result, a better understanding of HCMV immune evasion mechanisms could aid in the development of novel treatments and vaccines that are urgently required (9).

Natural killer (NK) cells are lymphocytes belonging to the innate immune system, first characterized for their ability to kill cancer cells with no prior sensitization (12). NK cells constitute a primary line of defence against virally infected cells, tumor cells, fungi and bacteria. They play a major role in controlling HCMV infection, as NK cell-deficient patients suffer lethal HCMV infections (13). NK cell activation is governed by a balance of signals

transduced by activating and inhibitory receptors (14). When the balance tips in favour of activation, NK cells kill the target cells and secrete cytokines and chemokines that modulate the immune response (15).

A major activating receptor expressed on all NK cells is NKG2D, a c-type lectin that binds a family of eight stress induced ligands: MHC class I polypeptide-related sequences (MIC) A and B, and UL16 binding proteins (ULBP) 1–6 (16). Healthy cells usually do not express these ligands, but they can be induced by different stresses including heat shock, DNA damage and viral infection (17).

MICA is the most polymorphic stress-induced ligand, with >150 known alleles encoding >90 different MICA proteins (http://hla.alleles.org/nomenclature/stats.html). Interestingly, the most prevalent MICA allele, MICA*008, contains a single nucleotide insertion in its transmembrane domain, giving rise to a short frameshifted sequence terminated by a premature stop codon. This truncated allele is first synthesized in a soluble form, but then becomes tethered to the membrane by a glycosylphosphatidylinositol (GPI) anchor, through a slow and poorly characterized nonstandard maturation pathway (18). In contrast, all other MICA alleles are membrane-spanning proteins with a cytosolic tail. As a result, MICA*008 has unique biological properties, including different apical/basolateral sorting, preferential lipid raft localization and release by exosomes (18,19). MICA*008 has been implicated in autoimmune disease, transplant rejection and cancer immune evasion (19–22).

HCMV targets the NKG2D stress-induced ligands by multiple and diverse immune evasion mechanisms, including by manipulation of the ubiquitin proteasome system (23–25). The viral microRNA miR-UL112 inhibits MICB translation (26). The viral protein UL16

sequesters MICB, ULBP1, ULBP2 and ULBP6 in the ER (27–31). The viral MHC homologue UL142 retains MICA and ULBP3 in the *cis*-Golgi apparatus (32–34). The viral proteins US18 and US20 jointly target MICA to lysosomal degradation, while US12, US13 and US20 jointly target ULBP2 and MICB (35–37). Similarly, the viral protein UL148A induces the lysosomal degradation of MICA together with an unknown viral interaction partner (38).

Notably, MICA*008 is unaffected by these mechanisms, which gave rise to the hypothesis that it is highly prevalent due to the evolutionary advantage it confers (39). However, we have previously found that the HCMV protein US9 specifically targets MICA*008 to proteasomal degradation, suggesting that HCMV has evolved counter-measures to this common allele. While studying US9-deficient HCMV, we discovered that MICA*008 is targeted by additional, as-yet unidentified HCMV factors, since even the US9-deficient virus could still downregulate MICA*008 to a certain degree (40).

UL147A is a 75 amino acid early-late HCMV protein that is unnecessary for viral replication and has no known function (41,42). UL147A has a predicted N-terminal signal peptide, a predicted transmembrane domain at its C-terminus and no predicted glycosylation sites (https://www.uniprot.org/uniprot/F5H8R0) (43). It is encoded in the UL*b′* region located at the right end of the unique long HCMV genomic segment. This 13–15 kbp region encompassing the UL133–UL150 genes is known to encode multiple immune evasion factors (32,33,50,38,39,44–49) and is present in clinical HCMV isolates but is frequently lost during serial passaging in fibroblast cell culture (7,42,51–54). However, UL147A is highly conserved in clinical isolates with a maximum of 6–7% sequence variability (41). Here, we

116 show that UL147A specifically targets MICA*008 to proteasomal degradation, resulting in

117 reduced NK-cell mediated killing of HCMV-infected cells.

Results

*UL147A-deficient HCMV mutants are impaired in MICA*008 downregulation*

Since the UL*b'* region of the HCMV genome contains genes that target full-length MICA alleles, we hypothesized that this region might also contain MICA*008-targeting genes. To search for such genes, VH3 human foreskin fibroblasts (HFF) that are MICA*008 homozygous (40) were mock infected, or infected with two variants of the HCMV strain AD169: AD169VarS (VarS), or a bacterial artificial chromosome (BAC)-cloned AD169VarL (55), named BAC2. BAC2 contains most of the UL*b'* genomic region except for a UL140–144 deletion, while VarS completely lacks UL*b'*. At 96 hours post-infection (hpi), MICA*008 surface expression was assayed by flow cytometry (Fig. 1A). Interestingly, MICA*008 surface levels were upregulated following infection with VarS, but not with BAC2. This suggested that the UL*b'* region encodes at least one MICA*008-targeting gene.

To ascertain which UL*b'* gene(s) were responsible for the observed phenotype, we utilized an array of block and single-gene deletion mutants generated on the BAC2 background (38,48) (Fig. 1B). For this screen, we used MRC-5 human lung fibroblasts (HLFs) which we genotyped and determined to be MICA*008 homozygous. We assayed MICA surface expression by flow cytometry at 72 hpi. Initially, MRC-5 HLFs were infected with BAC-cloned VarS (termed BAC20), BAC2 or five different BAC2 block deletion mutants, to narrow our region of interest (Fig. 1C, quantified in Fig. 1D). Two of the block deletion mutants were impaired in MICA*008 downregulation, similarly to BAC20: BAC2 ΔUL146-148, and the larger BAC2 ΔUL133-148 deletion that contains the UL146-148 deletion within it. In contrast, infection with BAC2 ΔUL133-139, BAC2 ΔUL148A-D and BAC2 ΔUL149-

150 reduced MICA*008 surface expression to a similar extent as parental BAC2. We therefore focused on the UL146-148 genes for further analysis.

To identify the specific MICA*008-targeting gene(s), we generated BAC2 single deletion mutants of the four genes in this block: ΔUL146, ΔUL147, ΔUL147A and ΔUL148. We infected MRC-5 HLFs with BAC2, BAC20 and the single deletion mutants, and assayed MICA*008 surface expression at 72 hpi (Fig. 1E, quantified in Fig. 1F). Of the four single deletion mutants, only BAC2 ΔUL147A was impaired in MICA*008 downregulation, similarly to BAC20. We therefore concluded that UL147A was the UL*b'* gene required for MICA*008 downregulation.

*Total MICA*008 protein quantity is reduced by UL147A overexpression*

We next wanted to determine if UL147A is sufficient for MICA*008 downregulation. We cloned UL147A fused to an N-terminal FLAG tag that was inserted after its endogenous signal peptide. We transduced an empty vector (EV) control or the UL147A-FLAG construct into 293T cells (MICA*008 homozygous) or HCT116 cells (MICA*001/*009:02 full-length alleles) (56,57). We then measured MICA surface expression by flow cytometry (Fig. 2A). MICA*008 surface expression was significantly downregulated in UL147A-overexpressing 293T cells compared to EV controls, but there was no difference in MICA levels in HCT116 cells. This lack of effect on full-length MICA alleles matches our previous results, since we showed that the ΔUL146-148 block deletion mutant was not impaired in full-length MICA downregulation (38).

Next, we lysed the transfected cells and performed a western blot to visualize UL147A (Fig. 2B). In both cell types, UL147A migrated as a single band of 12-13 kDa. We then assessed

UL147A's effect on total MICA quantity. MICA is a highly glycosylated protein that migrates as a 'smear' of differentially glycosylated forms in western blots (40). Importantly, whole-cell MICA*008 quantity was markedly reduced in 293T-UL147A cells, with no effect in HCT116-UL147A cells (Fig. 2C). This suggested that the UL147A-mediated reduction in surface MICA*008 was not due to intracellular sequestration, but rather due to a reduction in total protein quantity.

We confirmed these results in RKO cells transduced with an EV, MICA*004-HA or MICA*008-HA. RKO cells endogenously express very low levels of intracellular MICA*007:01 and hence are a useful model for comparing exogenously expressed MICA alleles (40). The various RKO cells were transduced with an EV control or with UL147A-FLAG, and MICA surface expression was measured by FACS staining (Fig. 2D). Here too, only MICA*008 was downregulated by UL147A while MICA*004 remained unchanged. We also stained the RKO MICA*008 cells for other NKG2D ligands and for MHC class I (Fig. S1) and found that they were unaffected by UL147A, suggesting it is MICA*008-specific. Notably, a similar lack of effect of the UL*b'* region on other NKG2D ligands was previously observed during HCMV infection (38).

Next, we lysed the transfected RKO cells and performed a western blot analysis of UL147A expression (Fig. 2E) and of total MICA quantity (Fig. 2F). As with endogenous MICA, there was a substantial overall decrease in MICA*008 quantity and no effect was observed on MICA*004. However, not all MICA*008 forms were equally affected by UL147A (Fig. 2F, forms indicated by arrows). A ~70 kDa band vanished, while a ~60 kDa band remained unchanged. A similar effect can be seen in the UL147A-expressing 293T cells (Fig. 2C) but it is harder to appreciate since different MICA*008 forms migrate closely to each other in 293T

cells. The sparing of certain MICA*008 protein forms indicated that UL147A affects MICA*008 at some point following its translation.

In RKO cells, different MICA*008 maturation stages can be distinguished relatively easily, since N-linked glycosylations first added at the ER are modified and expanded during passage through the Golgi apparatus, and the resulting increase in glycoprotein size is prominent compared to other cell types (40). We therefore speculated that the differently sized UL147A-susceptible and UL147A-resistant MICA*008 forms correspond to different stages of MICA*008 maturation.

To directly identify the UL147A-resistant MICA*008 form, we performed an endoglycosidaseH (endoH) sensitivity assay. EndoH only removes unmodified N-linked glycosylations prior to glycoprotein passage through the Golgi apparatus, while PNGaseF removes all N-linked glycosylations. We digested lysates obtained from RKO MICA*008-HA cells expressing an EV or UL147A-FLAG (Fig. 2G). In EV-expressing cells, most of MICA*008 was in the highly glycosylated ~70 kDa form, which was endoH-resistant. Only the minor, ~60 kDa band was endoH sensitive. Notably, following deglycosylation, the endoH-resistant form migrated more rapidly at ~34 kDa compared to the endoH-sensitive form which migrated at ~37 kDa. This apparent size difference is due to the presence of the GPI anchor in the mature, endoH-resistant form of MICA*008, which increases the negative charge of the glycoprotein (18).

In contrast, in UL147A-FLAG expressing cells, only the ~60 kDa endoH-sensitive form remained, indicating ER-resident MICA*008 is the UL147A-resistant form. UL147A's relative sparing of the ER-resident form could indicate that MICA*008 is being degraded just before or just after it exits the ER, or alternately, that MICA*008 is diverted from the

208 secretory pathway and therefore fails to pass through the Golgi apparatus.

209 ***UL147A is an ER-resident protein which reduces surface MICA*008 but spares ER-***

210 ***resident MICA*008***

211 To directly visualize UL147A's effect on MICA*008 and determine the cellular localization

212 of both proteins, we utilized immunofluorescence. We fixed and permeabilized RKO

213 MICA*008-HA cells expressing either an EV control or UL147A-FLAG and stained them

214 for the ER marker protein disulfide isomerase (PDI), for MICA and for FLAG-tag (Fig. 3A).

215 Nuclei were counterstained with DAPI. Interestingly, UL147A co-localized extensively with

216 PDI, indicating it is ER-resident. As for MICA*008, in EV-expressing cells, it resided mostly

217 at the cell surface with a fraction co-localizing with the ER marker PDI. However, in

218 UL147A-expressing cells, surface MICA*008 all vanished, and the remaining intracellular

219 MICA*008 overlapped PDI, indicating UL147A-resistant MICA*008 was ER-resident.

220 These results strengthen our findings from the endoH sensitivity assay (Fig. 2G) since they

221 demonstrate that mature MICA*008 is UL147A-susceptible. Importantly, these results also

222 rule out the possibility of altered MICA*008 subcellular localization, suggesting it is being

223 degraded at some point along its maturation pathway.

224 ***UL147A targets ER-resident MICA*008 to proteasomal degradation prior to the GPI-***

225 ***anchoring step***

226 Our results suggested that UL147A is ER-resident and that it induces MICA*008

227 degradation. To test whether UL147A targets MICA*008 to lysosomal or to proteasomal

228 degradation, we performed a cycloheximide (CHX) chase assay in the presence of lysosomal

229 and proteasomal inhibitors. CHX globally inhibits protein translation, facilitating the study of

230 protein degradation rates. RKO MICA*008-HA cells expressing either an EV control (Fig.

3B) or UL147A-FLAG (Fig. 3C) were left untreated or treated for 8 hours with CHX, in combination with the proteasomal inhibitors epoxomicin (EPX) or bortezomib (BTZ), or the lysosomal inhibitors leupeptin (LEU) or concanamycin A (CCMA). For each inhibitor, the appropriate vehicle-only mock treatment was matched.

In UL147A-expressing cells (Fig. 3C), even after 8 hours of CHX treatment, ER-resident MICA*008 remained detectable, demonstrating slow degradation kinetics. Importantly, treatment with proteasomal inhibitors resulted in the significant accumulation of a ~37 kDa form of MICA*008, which represents a deglycosylated cytosolic degradation intermediate which is not GPI anchored, based on its size (40). In contrast, lysosomal inhibitors did not affect MICA*008 levels. The same degradation intermediate was faintly visible in EV-expressing controls treated with EPX or BTZ (Fig. 3B), suggesting that low levels of MICA*008 were directed to proteasomal degradation even in UL147A's absence. We therefore concluded that UL147A directs MICA*008 to degradation in the proteasome after a prolonged lag in the ER, but prior to the GPI-anchoring step and ER exit.

Lastly, we wondered whether UL147A-induced proteasomal degradation of MICA*008 was mediated directly or indirectly. We performed an anti-FLAG-tag co-immunoprecipitation in RKO MICA*008 cells, followed by immunoblotting for FLAG-tag and MICA (Fig. S2). We found that the ER-resident form of MICA*008 (shown by a black arrow) co-precipitated with UL147A, supporting a direct interaction between the two.

*Specific MICA*008 features are required for UL147A-mediated downregulation*

We next wondered which MICA*008 features mediate UL147A's specificity to this allele. MICA*008 has two features distinguishing it from full-length MICA alleles: a frameshifted

sequence of 15 amino acids, and a premature stop codon that terminates this sequence. We previously generated RKO cells transduced with MICA*004 mutants modified with different MICA*008 sequence features (40) (Fig. 4A). In MICA*004-G-ins-HA, the G-nucleotide insertion of MICA*008 was introduced into the TM domain of MICA*004, and therefore this construct contains the 15 frameshifted amino acids and the premature stop codon. MICA*004-stop-HA only contains the premature stop codon at the same position as MICA*004-G-ins-HA. MICA*004-Dmut-HA is a double-mutated MICA*004. It includes the G-nucleotide insertion, but this insertion is corrected by a compensatory insertion after the 15 amino acid sequence, to restore the reading frame for the full remaining length of the MICA*004 allele. As a result, this allele has the frameshifted 15 amino acid sequence but not the premature stop codon. We previously found that only MICA*004-G-ins becomes GPI-anchored like MICA*008 (40). To address the role of the GPI anchor, we previously generated a MICA*008 mutant named MICA*008-ULBP3TM-HA, in which we swapped the transmembrane domain with that of ULBP3, another NKG2D ligand that contains a canonical GPI-anchoring signal. This mutant is also GPI-anchored, but via the rapid, canonical pathway (40).

RKO cells were transduced with an EV control or with the various MICA constructs, and then co-transduced with an EV control or with UL147A-FLAG. Construct surface expression was measured by flow cytometry (Fig 4B). Intriguingly, of all the MICA mutants, UL147A downregulated only MICA*004-G-ins. This suggests that both the frameshifted sequence and the premature stop codon are required for UL147A-mediated effect. Both features together are also required for MICA*008 GPI anchoring. However, canonical GPI anchoring was not sufficient for UL147A recognition, since MICA*008-ULBP3TM levels were unaffected by

UL147A. Taken together with the finding that MICA*008 degradation occurs before it becomes GPI-anchored, these results suggest that UL147A-mediated downregulation depends on MICA*008's non-canonical maturation pathway but not on the presence of the GPI anchor itself (40).

Having shown that the frameshifted sequence and premature stop codon were required features for UL147A recognition of MICA, we wanted to test whether they are also sufficient for UL147A recognition in the context of a different protein: MICB, which is not targeted by UL147A. 293T cells, which lack endogenous MICB surface expression, were transduced with an EV control, WT MICB, or with MICB-mut where the endogenous MICB TM domain was swapped with the MICA*008 TM domain (Fig. 4C) (40). We then co-transduced the 293T cells with an EV control or with UL147A-FLAG, and assessed MICB surface expression using flow cytometry. Native MICB was unaffected by UL147A, but the mutant bearing MICA*008's TM domain was substantially downregulated by it (Fig. 4D). This shows that MICA*008's TM domain is sufficient for conferring UL147A susceptibility.

UL147A-mediated MICA*008 downregulation leads to reduced NK-mediated killing of HCMV-infected cells

After characterizing UL147A's mechanism of action in an overexpression system, we wanted to assess its interactions with US9 and functional significance during HCMV infection. In addition to the UL147A and US9 single deletion mutants on the BAC2 background, we also wanted to study a deletion mutant lacking both proteins. We therefore generated a US9 deletion mutant on the BAC20 background that lacks the entire UL*b'* region and therefore lacks UL147A, as we have shown that UL147A is the only MICA*008-targeting gene in this region (Fig. 1E). MRC-5 HLFs were mock-infected or infected with BAC2, BAC2

299 ΔUL147A, BAC2 ΔUS9, BAC20 and BAC20 ΔUS9. A time course assay was performed to
300 track MICA*008 surface levels at 24, 48 and 72 hpi by flow cytometry (Fig. 5A, quantified
301 in Fig. 5B). All viruses led to the upregulation of MICA*008 at 24 hpi to a similar extent
302 compared to the mock-infected control. At 48 hpi, only BAC20 ΔUS9-infected cells showed
303 markedly increased MICA*008 levels compared to cells infected with the other viruses. At
304 72 hpi, cells infected with BAC2 ΔUS9, BAC2 ΔUL147A or BAC20 showed a two-to-three-
305 fold increase in MICA*008 levels compared to BAC2-infected cells. BAC20 ΔUS9-infected
306 cells increased MICA*008 levels by about sevenfold compared to BAC2-infected cells.
307 These results show that UL147A has a similar effect magnitude and timing to that of US9 on
308 MICA*008 surface expression, and that deletion of the two together has an additive effect
309 during infection.

310 Since additional variables such as relative protein abundance or differences in expression
311 kinetics can influence protein effects during HCMV infection, we further tested the effect of
312 co-expressing US9 and UL147A together in an overexpression model, providing stable and
313 high levels of both proteins. RKO MICA*008-HA cells were transduced with an EV control,
314 US9-HIS (described in 39), UL147A-FLAG, or co-transduced with both UL147A and US9.
315 MICA*008 surface levels were then measured by flow cytometry (Fig. S3A, quantified in
316 Fig. S3B). There was no significant difference in MICA*008 levels between cells expressing
317 US9 alone, UL147A alone, or the two proteins together. We concluded that in contrast to
318 their additive effect on MICA*008 during infection, US9 and UL147A were functionally
319 redundant in an overexpression system.

320 Finally, we asked whether the increase in MICA*008 surface expression in BAC2
321 ΔUL147A-infected cells would affect NK cell-mediated killing. We performed a killing assay

322 in which MRC-5 HLFs were mock-infected or infected with BAC2, BAC2 ΔUL147A or
323 BAC2 ΔUS9. BAC20 and BAC20 ΔUS9 were excluded from this experiment due to the
324 absence of many additional UL*b'*-encoded NK-cell immune evasion functions in these
325 strains, which precludes comparison with the BAC2 single mutants. Infected cells were
326 labelled with radioactive ^{35}S, harvested at 72 hpi, and co-incubated with primary bulk
327 activated NK cells. MRC-5 cells infected with parental BAC2 were killed significantly less
328 than mock-infected cells (Fig. 5C). This reduction in NK-mediated killing was partially
329 reversed by the deletion of UL147A or of US9, with no significant difference between the
330 two mutants. This indicates that the similar MICA*008 upregulation caused by these
331 deletions was reflected by a comparable increase of NK-cell mediated killing, confirming
332 UL147A functionality during HCMV infection.

Discussion

In this study, we identified UL147A as a MICA*008-specific HCMV immunoevasin, in addition to US9. UL147A is the third MICA-targeting gene discovered in the UL*b′* region after UL142 and UL148A (45), and the fact that three out of six known MICA-targeting genes reside in this region emphasizes its importance for NK cell immune evasion.

Here, we show that UL147A directs MICA*008 to proteasomal degradation. It acts during MICA*008's prolonged and non-canonical maturation process, prior to the GPI-anchoring process (see model in Fig. 6). In this respect, UL147A and US9 share considerable functional homology – both degrade MICA*008 with slow kinetics and require MICA*008 non-canonical GPI-anchoring for recognition. Despite this, UL147A and US9 are encoded in different parts of the HCMV genome and share no significant structural similarity. The only structural feature they have in common is the presence of a short poly-serine stretch in their ER-luminal domains. This implies that the two proteins use different structural elements to induce similar effects. Interestingly, both proteins are also highly conserved in clinical HCMV strains (41,58). Future studies might utilize the two proteins to uncover MICA*008's poorly-characterized maturation pathway by seeking cellular interaction partners the two have in common, and thereby also shed light on the mechanistic significance of these structural differences.

The lack of additive or synergistic interaction between UL147A and US9 in an overexpression system supports the concept that both proteins share a similar target, probably one related to the non-canonical MICA*008 maturation pathway. Their additivity during infection might be due to lower levels of expression as compared to the overexpression system, so that neither protein attains its peak effect.

Other examples of multiple HCMV immunoevasins targeting a single ligand show complementary mechanisms of action and temporal patterns, aiding in effective suppression of the targeted ligand (24). However, this is not the case with UL147A and US9, as both are similar in terms of function and temporal activity. While more subtle differences in their mechanism of action may be discovered in the future, another possible explanation for this apparent redundancy is that US9 and UL147A have additional, non-overlapping functions. It was recently shown that US9 also interferes with the STING and MAVS pathways to evade type I interferon responses (59). A recent proteomic study of the HCMV interactome (4) identified distinct lists of US9 and UL147A interactors. It would therefore be interesting to assess UL147A's ability to regulate other known US9 targets, and to search for additional, unknown targets.

HCMV encodes multiple mechanisms that target MICA: UL142, US18, US20 and UL148A for full-length MICA alleles, and US9 and UL147A for MICA*008 (32,33,35,38,40). All MICA-targeting mechanisms discovered to date follow a strict dichotomy: full-length allele-targeting or MICA*008-targeting, and UL147A also follows this rule. The division is also maintained with regard to the mechanism of MICA degradation – preferentially lysosomal degradation for full-length alleles versus proteasomal degradation for MICA*008. This division supports the notion that the different mechanisms of degradation might be related to the different biological features of MICA*008 and full-length MICA alleles.

Until recently, MICA*008 was considered an 'escape variant' resistant to MICA-targeting HCMV mechanism (39). However, we found that US9, and now UL147A, specifically target this prevalent allele. The fact that MICA*008 is targeted by multiple HCMV mechanisms

stresses its importance for HCMV biology, and additional MICA*008-targeting mechanisms may be discovered in the future.

MICA itself is only conserved in certain great apes (60), and the truncated mutant MICA*008 is unique to humans (61). We previously postulated that some of the HCMV mechanisms targeting full-length alleles appeared earlier in CMV evolution, and that following MICA*008's appearance and increasing prevalence, HCMV evolved newer mechanisms to counter this allele (40). UL147A, which is only conserved in certain great ape CMV, is indeed more recent than US18/20. However, so are full-length-MICA specific UL148A and UL142 (35,42,62). This indicates continuing evolution of mechanisms that target both full-length MICA alleles and MICA*008.

Another intriguing point to consider is that conserved CMV immune evasion genes may have divergent targets in different species. It was recently shown that the rhesus CMV gene Rh159 intracellularly retains several simian NKG2D ligands and can also retain human MICA (63). However, its HCMV homolog, UL148, instead targets CD58 (50,63). Possibly, UL148 was repurposed as new genes that target the NKG2D ligands arose. It is therefore also possible that MICA*008-targeting genes including UL147A, were also repurposed or gained additional MICA*008-targeting functionality, since their appearance predates that of MICA*008.

In summary, the discovery of UL147A's immune evasion function expands our understanding of the complex and rapidly shifting virus-host interactions which shaped the evolution of the NKG2D ligands.

Materials and methods

Cells. The 293T (CRL-3216), HCT116 (CCL-247), RKO (CRL-2577) cell lines were obtained from the ATCC. MRC-5 (CCL-171) primary human lung fibroblasts were also obtained from the ATCC, and VH3 primary human foreskin fibroblasts were obtained from a healthy donor and were previously described (64). All fibroblasts were used below passage 21. All cell lines and fibroblasts were kept in Dulbecco's modified Eagle's medium, except for MRC-5 cells that were kept in Eagle's minimum essential medium (Biological Industries). Media were supplemented with 10% (vol/vol) fetal calf serum (Sigma-Aldrich) and with 1% (vol/vol) each of penicillin-streptomycin, sodium pyruvate, L-glutamine and nonessential amino acids (Biological Industries). NK cells were isolated from peripheral blood lymphocytes and activated as previously described (65). NK purity was >95% by FACS analysis. All primary cells were obtained in accordance with the institutional guidelines and permissions for using human tissues.

Antibodies. The following primary antibodies were used for flow cytometry: anti-MICA (clone 159227; R&D Systems) and anti-MICB (clone 236511, R&D Systems).

The following primary antibodies were used for immunofluorescence: anti-PDI (ab3672, Abcam), anti-FLAG tag (Clone L5, Biolegend) and anti-MICA (clone 159227, R&D Systems).

The following primary antibodies were used for western blotting: anti-MICA (Clone EPR6568, Abcam), anti-FLAG tag (Clone L5, Biolegend), anti-GAPDH (clone 6C5, Santa Cruz) and anti-vinculin (clone EPR8185, Abcam).

The following secondary antibodies were used: anti-mouse AlexaFluor 647, anti-mouse PE, anti-mouse biotin, anti-rabbit biotin, streptavidin-AlexaFluor 647, streptavidin-horseradish peroxidase (HRP), anti-mouse-HRP, anti-rat-HRP and anti-rabbit-HRP, all purchased from Jackson Laboratories.

Viruses and infection. AD169VarS and AD169VarL were isolated and cloned into BAC2 and BAC20 as previously described (55). BAC2-generated UL*b'* block deletion mutants were previously described (48).

Recombinant BAC2 single deletion mutants were generated according to previously published procedures (66,67). Briefly, a PCR fragment was generated (data not shown) using plasmid pSLFRTKn (68) as the template DNA. The PCR fragments containing a kanamycin resistance gene were inserted into the parental AD169-BAC2 strain (55) by homologous recombination in Escherichia coli. The inserted cassette replaces the target sequence which was defined by flanking sequences in the primers. Recombinant HCMVs were reconstituted from HCMV BAC DNA by Superfect (Qiagen) transfection into permissive MRC-5 cells.

HFFs were used to propagate all HCMV strains and virus stocks were titrated using a plaque assay and stored at -80°C. Infection with the various virus strains was carried out at a multiplicity of infection (MOI) of 2-4, in confluent fibroblasts. HCMV infection was enhanced by centrifugation at 800 g for 30 min.

To verify infection efficiency, the fraction of HCMV-infected cells was assessed by intracellular flow cytometry at 24 hpi. Cells were stained with 0.25 µg/well of an AlexaFluor 488-conjugated anti-CMV-immediate-early antibody (clone 8B1.2; Sigma-Aldrich), and samples were used only if >75% infected and if the variance between samples was <15%.

MICA Genotyping. MICA genotyping was performed as previously described (40). Briefly, genomic DNA was extracted using the AccuPrep genomic DNA extraction kit (Bioneer) according to the manufacturer's instructions. The area including MICA exons 2-5 was amplified, ligated into pGEM T-easy plasmids (Promega) and sent for sequencing. Homozygosity was determined by at least four separate sequencings.

Vectors and primers used for cloning. Generation of the MICA and MICB constructs was previously described (40). Briefly, sequences were amplified from cDNA of cell lines with the appropriate genotype. Where relevant, site-directed PCR mutagenesis was used to generate MICA and MICB mutants. Sequences were then inserted into lentiviral vector SIN18pRLL-hEFIap-E-GFP-WRPE, replacing the green fluorescent protein (GFP) reporter.

UL147A was cloned from cDNA derived from cells infected with AD169 VarL HCMV strain with the preceding intron sequence, to increase expression levels. To insert a FLAG-tag after the endogenous signal peptide, 3 sequential PCR reactions were carried out, with reaction 3 unifying the PCR fragments from reactions 1 and 2 using reaction 1 forward and reaction 2 reverse primers.

The following primers were used for cloning UL147A:

Reaction 1 forward – 5'- CCGCGGCCGCGCCGCCACCTGGAGGCCTAGGCTTTTGC-3' and reaction 1 reverse – 5'-AATCTCCTTGTCGTCATCGTCTTTGTAGTCTGCGAGGATACTAGTGCTATACCA-3'.

reaction 2 forward – 5'-GACTACAAAGACGATGACGACAAGGAGATTAACGAAAACTCCTGCTC-3' and reaction 2 reverse – 5'-ggCTCGAGTCAGATCACACAAGTGACGAGGAG-3'

464 The resultant amplified fragment was cloned into the lentiviral vector pHAGE-DsRED(−)-
465 eGFP(+), which also contains GFP, using the restriction enzymes NotI and XhoI.

466 ***Lentivirus production and transduction***. Lentiviral vectors were produced in 293T cells
467 using TransIT-LT1 transfection reagent (Mirus) for a transient three-plasmid transfection
468 protocol as previously described (26). Cells were transduced in the presence of Polybrene (6
469 μg/ml). Transduction efficiency was evaluated by GFP levels, and only cell populations with
470 >90% GFP positive cells were used. If necessary, cells were sorted to achieve the required
471 efficiency.

472 ***Flow cytometry.*** For flow cytometry, cells were plated at equal densities and incubated
473 overnight. Cells were resuspended and incubated on ice with the primary antibody (0.2
474 μg/well) for 1 h, then incubated for 30 mins on ice with the secondary antibody (0.75
475 μg/well). 10,000 live cells were acquired from each sample. In certain experiments, 4′,6-
476 diamidino-2-phenylindole (DAPI) staining was used to exclude dead and dying cells. In all
477 experiments using cells transduced with a GFP-expressing lentivirus, the histograms shown
478 are gated on the GFP$^-$positive population.

479 ***Western blot***. Cells were plated at an equal density, incubated overnight, and lysed in buffer
480 containing 0.6% sodium dodecyl sulfate (SDS) and 10-mM Tris (pH 7.4) and the protease
481 inhibitors aprotinin and phenylmethylsulfonyl fluoride (each at 1:100 dilution). In certain
482 cases, lysates were digested with endoglycosidase H (endoH) or PNGaseF (NEB), according
483 to the manufacturer's instructions, prior to gel electrophoresis.
484 Lysates were then subjected to SDS polyacrylamide gel electrophoresis and transferred onto a
485 nitrocellulose membrane. The membrane was blocked in 5% skim milk–phosphate-buffered
486 saline (PBS)–Tween 20 for 1 h and then incubated with a primary antibody overnight,

washed 3 times in PBS-Tween 20, incubated with a secondary antibody for 0.5 h, and washed 3 times in PBS-Tween 20. Images were developed using an EZ-ECL kit (Biological Industries). Image Lab software (Bio-Rad) was used for quantification.

Cycloheximide chase assay and proteasome and lysosome inhibition. Cells were left untreated or incubated with 50 µg/ml cycloheximide (Sigma-Aldrich) for 8 h, in combination with mock treatment or with the following inhibitors: 100 µg/ml leupeptin (LEU; Merck Millipore), 20 nM concanamycin A (CCMA; Sigma-Aldrich), 8 µM epoxomicin (EPX; A2S), or 8 µM bortezomib (BTZ; LC Biolabs). Mock treatment consisted of an equivalent volume of the matching solvent. This experiment was conducted using cells expressing UL147A fused to an N-terminal 6XHis or FLAG-tag.

Immunofluorescence. Cells were grown on glass slides, then fixed and permeabilized in cold (−20°C) methanol. Cells were blocked overnight in CAS-block (Life Technologies) and then incubated overnight with primary antibodies diluted 1:50–200 in CAS block. The next day, cells were washed and incubated overnight in secondary antibodies diluted 1:500 in PBS containing 5% bovine serum albumin. Cells were then washed, treated for 5 min with DAPI, and covered with coverslips. A confocal laser scanning microscope (Zeiss Axiovert 200 M; Carl Zeiss MicroImaging) was used to obtain images, and images were processed using Olympus Fluoview FV1000 software.

NK cell killing assay. The cytotoxic activity of NK cells against HCMV-infected MRC-5 cells was assessed in ^{35}S release assays as described (65). NK cells were incubated with radioactively-labelled target cells for 5 hrs. The spontaneous release in all assays was always less than 50% of the total release and is subtracted from the calculation of the percentages of

509 killing. Percentages of killing were calculated as follows: (counts per minute [CPM] sample
510 − CPM spontaneous)/(CPM total − CPM spontaneous) × 100.

511 ***Statistical methods***. A one-way ANOVA was used to compare effects on MICA surface
512 expression (measured as normalized median fluorescent intensity) or to compare effects on
513 killing percentages. The ANOVA was considered statistically significant when $P<0.05$.
514 Where the ANOVA was statistically significant, a post-hoc contrasts test was conducted to
515 determine which mutants differed significantly from each other at alphas of 0.05 or 0.01. Full
516 statistical details including P values, F values, degrees of freedom and effect sizes (Cohen's
517 D) are presented in the relevant figures and figure legends.

518

519

520 **Acknowledgments**

521 This study was supported by the ISF Israel-China grant. Further support came from the GIF
522 foundation, the ICRF professorship grant, the Israeli Science Foundation (Moked), a Ministry
523 of Science Personal Medicine grant and the DKFZ-MOST grant, all to O.M. E.S. was
524 supported during her work by the Adams Fellowship Programme of the Israel Academy of
525 Sciences and Humanities and by the Foulkes Foundation. The funders had no role in study
526 design, data collection and interpretation, or the decision to submit the work for publication.

References

1. Griffiths P, Baraniak I, Reeves M. The pathogenesis of human cytomegalovirus. J Pathol. 2015 Jan;235(2):288–97.

2. Stern-Ginossar N, Weisburd B, Michalski A, Le VTK, Hein MY, Huang SX, et al. Decoding human cytomegalovirus. Science (80-). 2012 Nov;338(6110):1088–93.

3. Weekes MP, Tomasec P, Huttlin EL, Fielding CA, Nusinow D, Stanton RJ, et al. Quantitative temporal viromics: An approach to investigate host-pathogen interaction. Cell. 2014 Jun;157(6):1460–72.

4. Nobre L, Nightingale K, Ravenhill BJ, Antrobus R, Soday L, Nichols J, et al. Human cytomegalovirus interactome analysis identifies degradation hubs, domain associations and viral protein functions. Elife. 2019 Dec;8.

5. Nightingale K, Lin KM, Ravenhill BJ, Davies C, Nobre L, Fielding CA, et al. High-Definition Analysis of Host Protein Stability during Human Cytomegalovirus Infection Reveals Antiviral Factors and Viral Evasion Mechanisms. Cell Host Microbe. 2018 Sep;24(3):447-460.e11.

6. Bradley AJ, Lurain NS, Ghazal P, Trivedi U, Cunningham C, Baluchova K, et al. High-throughput sequence analysis of variants of human cytomegalovirus strains Towne and AD169. J Gen Virol. 2009 Oct;90(Pt 10):2375–80.

7. Gatherer D, Seirafian S, Cunningham C, Holton M, Dargan DJ, Baluchova K, et al. High-resolution human cytomegalovirus transcriptome. Proc Natl Acad Sci U S A. 2011 Dec;108(49):19755–60.

548 8. Van Damme E, Van Loock M. Functional annotation of human cytomegalovirus gene
549 products: an update. Front Microbiol. 2014 Jan;5(MAY):218.

550 9. Berry R, Watson GM, Jonjic S, Degli-Esposti MA, Rossjohn J. Modulation of innate
551 and adaptive immunity by cytomegaloviruses. Nature Reviews Immunology. Nature
552 Publishing Group; 2019.

553 10. Manicklal S, Emery VC, Lazzarotto T, Boppana SB, Gupta RK. The "Silent" global
554 burden of congenital cytomegalovirus. Clin Microbiol Rev. 2013 Jan;26(1):86–102.

555 11. Anderholm KM, Bierle • C J, Schleiss • M R, Schleiss MR. Cytomegalovirus
556 Vaccines: Current Status and Future Prospects. Drugs. 2016;76:1625–45.

557 12. Freud AG, Mundy-Bosse BL, Yu J, Caligiuri MA. The Broad Spectrum of Human
558 Natural Killer Cell Diversity. Immunity. 2017 Nov;47(5):820–33.

559 13. Mace EM, Orange JS. Emerging insights into human health and NK cell biology from
560 the study of NK cell deficiencies. Immunol Rev. 2019 Jan;287(1):202–25.

561 14. Moretta L, Biassoni R, Bottino C, Mingari MC, Moretta A. Human NK-cell receptors.
562 Vol. 21, Immunology Today. Elsevier Ltd; 2000. p. 420–2.

563 15. Abel AM, Yang C, Thakar MS, Malarkannan S. Natural killer cells: Development,
564 maturation, and clinical utilization. Vol. 9, Frontiers in Immunology. Frontiers Media
565 S.A.; 2018.

566 16. Lanier LL. NKG2D Receptor and Its Ligands in Host Defense. Cancer Immunol Res
567 [Internet]. 2015 Jun [cited 2017 Dec 10];3(6):575–82. Available from:
568 http://www.ncbi.nlm.nih.gov/pubmed/26041808

17. Raulet DH, Gasser S, Gowen BG, Deng W, Jung H. Regulation of ligands for the NKG2D activating receptor. Annu Rev Immunol [Internet]. 2013 [cited 2017 Dec 10];31:413–41. Available from: http://www.ncbi.nlm.nih.gov/pubmed/23298206

18. Ashiru O, López-Cobo S, Fernández-Messina L, Pontes-Quero S, Pandolfi R, Reyburn HT, et al. A GPI anchor explains the unique biological features of the common NKG2D-ligand allele MICA*008. Biochem J. 2013;454(2):295–302.

19. Fernández-Messina L, Reyburn HT, Valés-Gómez M. Human NKG2D-ligands: cell biology strategies to ensure immune recognition. Front Immunol. 2012 Jan;3(September):299.

20. Ashiru O, Boutet P. Natural killer cell cytotoxicity is suppressed by exposure to the human NKG2D ligand MICA* 008 that is shed by tumor cells in exosomes. Cancer Res. 2010;70(2):1–17.

21. Loureiro J, Ploegh HL. Antigen presentation and the ubiquitin-proteasome system in host-pathogen interactions. Adv Immunol. 2006 Jan;92:225–305.

22. Risti M, Bicalho M da G. MICA and NKG2D: Is there an impact on kidney transplant outcome? Vol. 8, Frontiers in Immunology. Frontiers Research Foundation; 2017. p. 179.

23. De Pelsmaeker S, Romero N, Vitale M, Favoreel HW. Herpesvirus Evasion of Natural Killer Cells. J Virol. 2018 Mar;92(11).

24. Halenius A, Gerke C, Hengel H. Classical and non-classical MHC i molecule manipulation by human cytomegalovirus: So many targets - But how many arrows in the quiver? Cell Mol Immunol. 2015 Nov;12(2):139–53.

591 25. Le-Trilling VTK, Trilling M. Ub to no good: How cytomegaloviruses exploit the
592 ubiquitin proteasome system. Vol. 281, Virus Research. Elsevier B.V.; 2020. p.
593 197938.

594 26. Stern-Ginossar N, Elefant N, Zimmermann A, Wolf DG, Saleh N, Biton M, et al. Host
595 immune system gene targeting by a viral miRNA. Science. 2007 Jul;317(5836):376–
596 81.

597 27. Dunn C, Chalupny NJ, Sutherland CL, Dosch S, Sivakumar P V, Johnson DC, et al.
598 Human cytomegalovirus glycoprotein UL16 causes intracellular sequestration of
599 NKG2D ligands, protecting against natural killer cell cytotoxicity. J Exp Med
600 [Internet]. 2003 Jun 2 [cited 2017 Dec 24];197(11):1427–39. Available from:
601 http://www.ncbi.nlm.nih.gov/pubmed/12782710

602 28. Welte SA a, Sinzger C, Lutz SZZ, Singh-Jasuja H, Sampaio KLL, Eknigk U, et al.
603 Selective intracellular retention of virally induced NKG2D ligands by the human
604 cytomegalovirus UL16 glycoprotein. Eur J Immunol. 2003 Jan;33(1):194–203.

605 29. Rölle A, Mousavi-Jazi M, Eriksson M, Odeberg J, Söderberg-Nauclér C, Cosman D, et
606 al. Effects of Human Cytomegalovirus Infection on Ligands for the Activating
607 NKG2D Receptor of NK Cells: Up-Regulation of UL16-Binding Protein (ULBP)1 and
608 ULBP2 Is Counteracted by the Viral UL16 Protein. J Immunol. 2003 Jul;171(2):902–
609 8.

610 30. Eagle RA, Traherne JA, Hair JR, Jafferji I, Trowsdale J. ULBP6/RAET1L is an
611 additional human NKG2D ligand. Eur J Immunol. 2009 Nov;39(11):3207–16.

612 31. Cosman D, Müllberg J, Sutherland CL, Chin W, Armitage R, Fanslow W, et al.

ULBPs, novel MHC class I-related molecules, bind to CMV glycoprotein UL16 and stimulate NK cytotoxicity through the NKG2D receptor. Immunity. 2001 Mar;14(2):123–33.

32. Ashiru O, Bennett NJ, Boyle LH, Thomas M, Trowsdale J, Wills MR. NKG2D ligand MICA is retained in the cis-Golgi apparatus by human cytomegalovirus protein UL142. J Virol [Internet]. 2009 Dec 1 [cited 2018 Jan 2];83(23):12345–54. Available from: http://www.ncbi.nlm.nih.gov/pubmed/19793804

33. Chalupny NJ, Rein-Weston A, Dosch S, Cosman D. Down-regulation of the NKG2D ligand MICA by the human cytomegalovirus glycoprotein UL142. Biochem Biophys Res Commun [Internet]. 2006 [cited 2017 Dec 10];346:175–181. Available from: https://samba.huji.ac.il/+CSCO+0075676763663A2F2F6E702E7279662D7071612E70627A++/S0006291X06011491/1-s2.0-S0006291X06011491-main.pdf?_tid=5d909e5c-dd96-11e7-b12c-00000aacb360&acdnat=1512902534_2727df31b736311f35a00e4c5b5c572e

34. Wills MRM, Ashiru O, Reeves MB, Okecha G, Trowsdale J, Tomasec P, et al. Human cytomegalovirus encodes an MHC class I-like molecule (UL142) that functions to inhibit NK cell lysis. J …. 2005 Dec;175(11):7457–65.

35. Fielding CA, Aicheler R, Stanton RJ, Wang ECY, Han S, Seirafian S, et al. Two novel human cytomegalovirus NK cell evasion functions target MICA for lysosomal degradation. PLoS Pathog [Internet]. 2014 May [cited 2017 Dec 10];10(5):e1004058. Available from: http://www.ncbi.nlm.nih.gov/pubmed/24787765

36. Fielding CA, Weekes MP, Nobre L V, Ruckova E, Wilkie GS, Paulo JA, et al. Control

of immune ligands by members of a cytomegalovirus gene expansion suppresses natural killer cell activation. Elife [Internet]. 2017 Feb 10 [cited 2017 Dec 24];6:e22206. Available from: https://elifesciences.org/articles/22206

37. Charpak-Amikam Y, Kubsch T, Seidel E, Oiknine-Djian E, Cavaletto N, Yamin R, et al. Human cytomegalovirus escapes immune recognition by NK cells through the downregulation of B7-H6 by the viral genes US18 and US20. Sci Rep. 2017;7(1).

38. Dassa L, Seidel E, Oiknine-Djian E, Yamin R, Wolf DG, Le-Trilling VTK, et al. The Human Cytomegalovirus Protein UL148A Downregulates the NK Cell-Activating Ligand MICA To Avoid NK Cell Attack. J Virol [Internet]. 2018 Sep 1 [cited 2018 Sep 15];92(17):e00162-18. Available from: http://www.ncbi.nlm.nih.gov/pubmed/29950412

39. Wilkinson GGWG, Tomasec P, Stanton RJ, Armstrong M, Prod'homme V, Aicheler R, et al. Modulation of natural killer cells by human cytomegalovirus. J Clin Virol. 2008 Mar;41(3):206–12.

40. Seidel E, Le VTK, Bar-On Y, Tsukerman P, Enk J, Yamin R, et al. Dynamic Co-evolution of Host and Pathogen: HCMV Downregulates the Prevalent Allele MICA*008 to Escape Elimination by NK Cells. Cell Rep. 2015;10(6):968–82.

41. Lurain N, Fox A, Lichy H, Bhorade S, Ware C, Huang D, et al. Analysis of the human cytomegalovirus genomic region from UL146 through UL147A reveals sequence hypervariability, genotypic stability, and overlapping transcripts. Virol J. 2006;3(1):4.

42. Davison AJ, Dolan A, Akter P, Addison C, Dargan DJ, Alcendor DJ, et al. The human cytomegalovirus genome revisited: comparison with the chimpanzee cytomegalovirus

genome. J Gen Virol. 2003 Jan;84(1):17–28.

43. Bateman A, Martin MJ, O'Donovan C, Magrane M, Alpi E, Antunes R, et al. UniProt: The universal protein knowledgebase. Nucleic Acids Res. 2017 Jan;45(D1):D158–69.

44. Wilkinson GWG, Davison AJ, Tomasec P, Fielding CA, Aicheler R, Murrell I, et al. Human cytomegalovirus: taking the strain. Vol. 204, Medical Microbiology and Immunology. Springer Verlag; 2015. p. 273–84.

45. Patel M, Vlahava VM, Forbes SK, Fielding CA, Stanton RJ, Wang ECY. HCMV-encoded NK modulators: Lessons from in vitro and in vivo genetic variation. Vol. 9, Frontiers in Immunology. Frontiers Media S.A.; 2018.

46. Smith W, Tomasec P, Aicheler R, Loewendorf A, Nemčovičová I, Wang ECY, et al. Human cytomegalovirus glycoprotein UL141 targets the TRAIL death receptors to thwart host innate antiviral defenses. Cell Host Microbe. 2013 Mar;13(3):324–35.

47. Tomasec P, Wang ECY, Davison AJ, Vojtesek B, Armstrong M, Griffin C, et al. Downregulation of natural killer cell-activating ligand CD155 by human cytomegalovirus UL141. Nat Immunol [Internet]. 2005 Feb [cited 2018 Jan 2];6(2):181–8. Available from: http://www.ncbi.nlm.nih.gov/pubmed/15640804

48. Le-Trilling VTK, Becker T, Nachshon A, Stern-Ginossar N, Schöler L, Voigt S, et al. The Human Cytomegalovirus pUL145 Isoforms Act as Viral DDB1-Cullin-Associated Factors to Instruct Host Protein Degradation to Impede Innate Immunity. Cell Rep. 2020 Feb;30(7):2248-2260.e5.

49. Stanton RJ, Prod'Homme V, Purbhoo MA, Moore M, Aicheler RJ, Heinzmann M, et al. HCMV pUL135 remodels the actin cytoskeleton to impair immune recognition of

679 infected cells. Cell Host Microbe. 2014 Aug;16(2):201–14.

680 50. Wang ECY, Pjechova M, Nightingale K, Vlahava VM, Patel M, Ruckova E, et al.
681 Suppression of costimulation by human cytomegalovirus promotes evasion of cellular
682 immune defenses. Proc Natl Acad Sci U S A. 2018 May;115(19):4998–5003.

683 51. Anzai T, Shiina T, Kimura N, Yanagiya K, Kohara S, Shigenari A, et al. Comparative
684 sequencing of human and chimpanzee MHC class I regions unveils insertions/deletions
685 as the major path to genomic divergence. Proc Natl Acad Sci U S A. 2003
686 Jun;100(13):7708–13.

687 52. Dolan A, Cunningham C, Hector RD, Hassan-Walker AF, Lee L, Addison C, et al.
688 Genetic content of wild-type human cytomegalovirus. J Gen Virol [Internet]. 2004
689 [cited 2017 Dec 10];85(5):1301–12. Available from:
690 http://www.microbiologyresearch.org/docserver/fulltext/jgv/85/5/1301.pdf?expires=15
691 12903655&id=id&accname=guest&checksum=E604D26BB0875A262D2D1F1F21F9
692 D68C

693 53. Cha T-A, Tom E, Kemble GW, Duke GM, Mocarski ES, Spaete RR. Human
694 Cytomegalovirus Clinical Isolates Carry at Least 19 Genes Not Found in Laboratory
695 Strains Downloaded from. Vol. 70, JOURNAL OF VIROLOGY. 1996.

696 54. Murphy E, Yu D, Grimwood J, Schmutz J, Dickson M, Jarvis MA, et al. Coding
697 potential of laboratory and clinical strains of human cytomegalovirus. Proc Natl Acad
698 Sci U S A [Internet]. 2003 Dec 9 [cited 2017 Dec 10];100(25):14976–81. Available
699 from: http://www.ncbi.nlm.nih.gov/pubmed/14657367

700 55. Le VTK, Trilling M, Hengel H. The cytomegaloviral protein pUL138 acts as

potentiator of tumor necrosis factor (TNF) receptor 1 surface density to enhance ULb'-encoded modulation of TNF-α signaling. J Virol [Internet]. 2011 Dec [cited 2017 Dec 18];85(24):13260–70. Available from: http://www.ncbi.nlm.nih.gov/pubmed/21976655

56. Zhang Y, Lazaro a M, Lavingia B, Stastny P. Typing for all known MICA alleles by group-specific PCR and SSOP. Hum Immunol. 2001 Jun;62(6):620–31.

57. McSharry BP, Burgert H-G, Owen DP, Stanton RJ, Prod'homme V, Sester M, et al. Adenovirus E3/19K promotes evasion of NK cell recognition by intracellular sequestration of the NKG2D ligands major histocompatibility complex class I chain-related proteins A and B. J Virol. 2008 May;82(9):4585–94.

58. Mandic L, Miller MS, Coulter C, Munshaw B, Hertel L. Human cytomegalovirus US9 protein contains an N-terminal signal sequence and a C-terminal mitochondrial localization domain, and does not alter cellular sensitivity to apoptosis. J Gen Virol. 2009 May;90(5):1172–82.

59. Choi HJ, Park A, Kang S, Lee E, Lee TA, Ra EA, et al. Human cytomegalovirus-encoded US9 targets MAVS and STING signaling to evade type i interferon immune responses. Nat Commun. 2018 Dec;9(1).

60. Kasahara M, Yoshida S. Immunogenetics of the NKG2D ligand gene family. Immunogenetics. 2012 Dec;64(12):855–67.

61. Pellet P, Vaneensberghe C, Debré P, Sumyuen MH, Theodorou I. MIC genes in non-human primates. Eur J Immunogenet. 1999;26(2–3):239–41.

62. Malouli D, Nakayasu ES, Viswanathan K, Camp DG, Chang WLW, Barry PA, et al.

723 Reevaluation of the Coding Potential and Proteomic Analysis of the BAC-Derived
724 Rhesus Cytomegalovirus Strain 68-1. J Virol. 2012 Sep;86(17):8959–73.

725 63. Sturgill ER, Malouli D, Hansen SG, Burwitz BJ, Seo S, Schneider CL, et al. Natural
726 Killer Cell Evasion Is Essential for Infection by Rhesus Cytomegalovirus. PLoS
727 Pathog. 2016 Aug;12(8).

728 64. Hengel H, Esslinger C, Pool J, Goulmy E, Koszinowski UH. Cytokines restore MHC
729 class I complex formation and control antigen presentation in human cytomegalovirus-
730 infected cells. J Gen Virol. 1995 Dec;76(12):2987–97.

731 65. Mandelboim O, Reyburn HT, Valés-Gómez M, Pazmany L, Colonna M, Borsellino G,
732 et al. Protection from lysis by natural killer cells of group 1 and 2 specificity is
733 mediated by residue 80 in human histocompatibility leukocyte antigen C alleles and
734 also occurs with empty major histocompatibility complex molecules. J Exp Med. 1996
735 Sep;184(3):913–22.

736 66. Tischer BK, von Einem J, Kaufer B, Osterrieder N. Two-step red-mediated
737 recombination for versatile high-efficiency markerless DNA manipulation in
738 Escherichia coli. Biotechniques [Internet]. 2006 Feb [cited 2017 Dec 25];40(2):191–7.
739 Available from: http://www.ncbi.nlm.nih.gov/pubmed/16526409

740 67. Wagner M, Gutermann A, Podlech J, Reddehase MJ, Koszinowski UH. Major
741 Histocompatibility Complex Class I Allele-specific Cooperative and Competitive
742 Interactions between Immune Evasion Proteins of Cytomegalovirus. J Exp Med. 2002
743 Sep;196(6):805–16.

744 68. Atalay R, Zimmermann A, Wagner M, Borst E, Benz C, Messerle M, et al.

745 Identification and Expression of Human Cytomegalovirus Transcription Units Coding

746 for Two Distinct Fc Receptor Homologs. J Virol. 2002;76(17):8596–608.

747

Figures

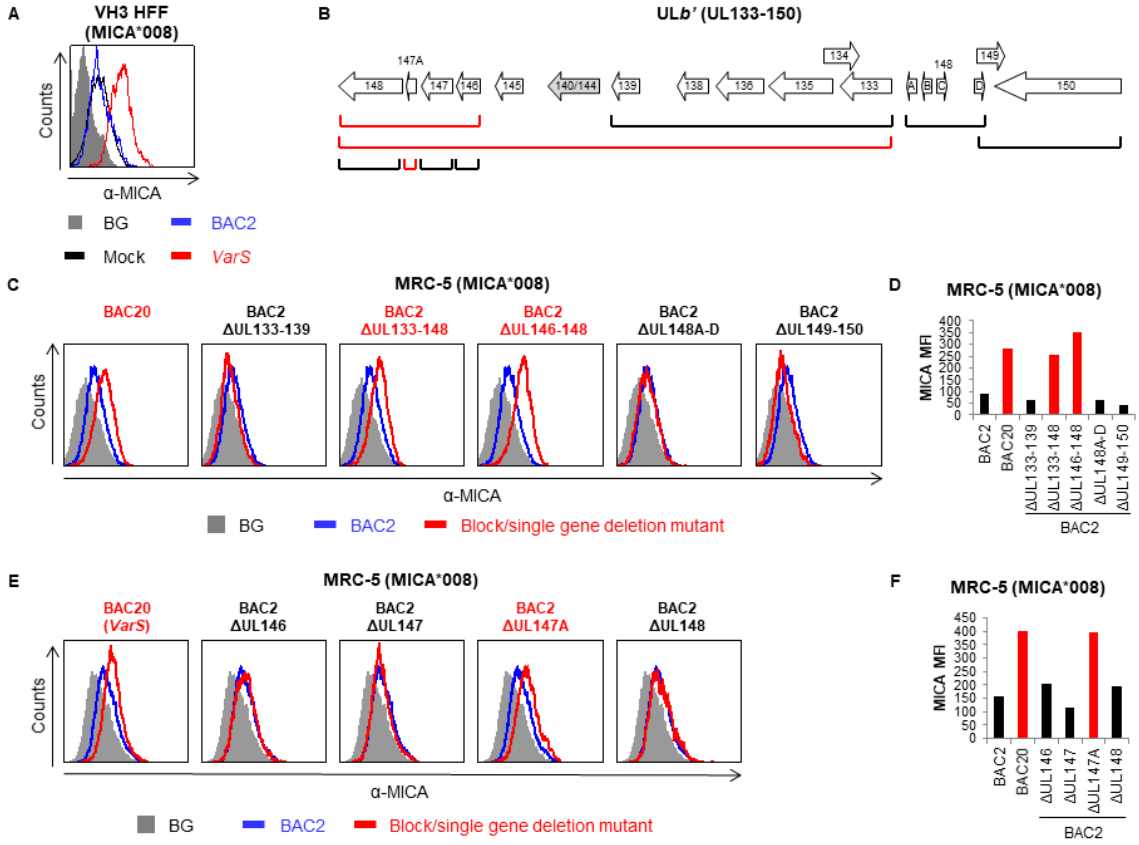

Figure 1. UL147A-deficient HCMV mutants are impaired in MICA*008 downregulation. (A) VH3 HFFs (MICA*008 homozygous) were either mock infected or infected with the indicated HCMV strains. Cells were harvested at 96 h post infection (hpi), and MICA surface expression was assayed by flow cytometry. Grey-filled histogram represents an isotype control staining of mock-infected cells, all control stainings were similar to the one shown. (B) Diagram of the UL*b'* genomic region (UL133–150). Brackets indicate block or single gene deletions generated on the BAC2 background. Red brackets indicate deletion mutants impaired in MICA*008 downregulation. (C-D) MRC-5 HLFs (MICA*008 homozygous) were either mock infected or infected with the indicated HCMV

759 strains. Cells were harvested at 72 h post infection (hpi), and MICA surface expression was
760 assayed by flow cytometry. Histograms are shown for block deletion mutants (C) and their
761 quantification (D) or for single gene deletion mutants (E) and their quantification (F). Grey-
762 filled histograms represent an isotype control staining of mock-infected cells, which was
763 similar to that of all other cells. Red font and bars highlight deletion mutants whose
764 phenotype matches that of UL*b'*-deficient virus.

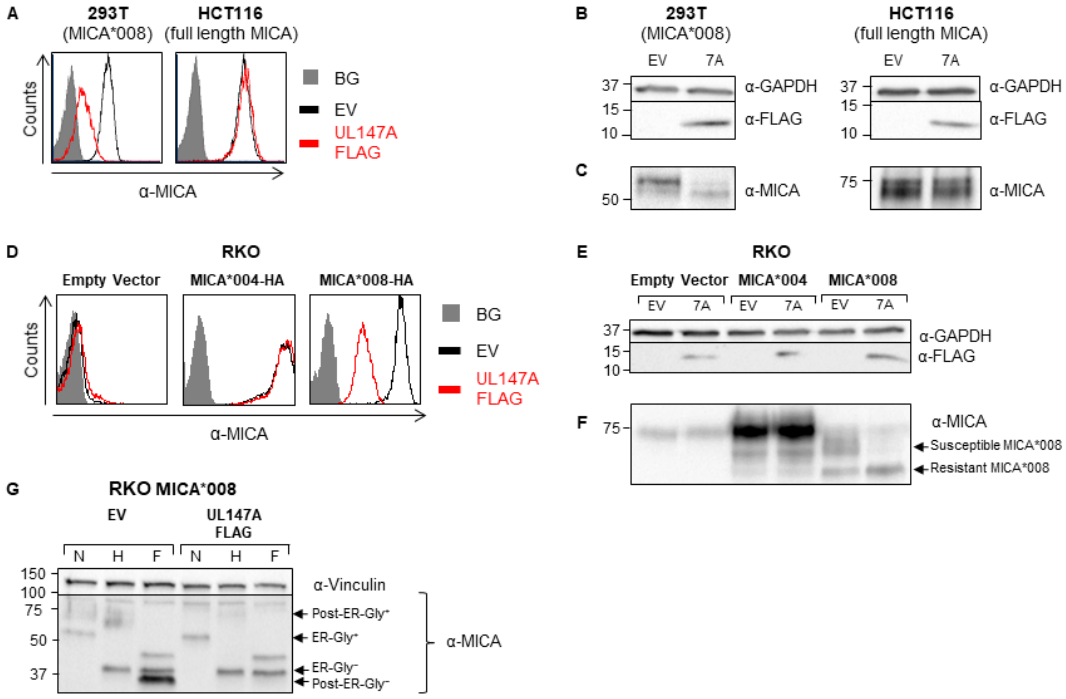

765

766 **Figure 2. Total MICA*008 protein quantity is reduced by UL147A overexpression.** (A)
767 293T (MICA*008 homozygous) and HCT116 (MICA*001/*009:02 full length alleles) were
768 transduced with an EV (black histograms) or with UL147A-FLAG (red histograms) and
769 MICA surface expression was assayed by flow cytometry. Gray-filled histograms represent
770 secondary antibody staining of EV cells, all control stainings were similar to the one shown.
771 Representative of three independent experiments. (B-C) The cells shown in (A) were lysed
772 and a western blot was performed using anti-MICA antibody for detection of MICA, anti-
773 FLAG tag antibody for detection of UL147A, and anti-GAPDH antibody as a loading
774 control. The lysates were split in two and run on two gels (shown separately in B, C) to
775 resolve proteins of different sizes. (D) RKO cells were transduced with an EV, with

776 MICA*004-HA or with MICA*008-HA, and then co-transduced with an EV or with
777 UL147A-FLAG. MICA surface expression was assayed by flow cytometry. Gray-filled
778 histograms represent secondary antibody staining of EV cells, all control stainings were
779 similar to the one shown. Representative of three independent experiments. (E-F) The cells
780 shown in (D) were lysed and a western blot was performed using anti-MICA antibody for
781 detection of MICA, anti-FLAG tag antibody for detection of UL147A, and anti-GAPDH
782 antibody as a loading control. The lysates were split in two and run on two gels (shown
783 separately in E, F) to resolve proteins of different sizes. Arrows indicate UL147A-susceptible
784 and UL147A-resistant forms of MICA*008. (G) RKO MICA*008-HA cells co-transduced
785 with EV or UL147A-FLAG were lysed. Lysates were left untreated or digested with endoH
786 or with PNGaseF (marked N, H and F, respectively), and then blotted using anti-MICA and
787 anti-vinculin as a loading control. Arrows indicate ER-resident (endoH sensitive) and post-
788 ER (endoH resistant) MICA*008 forms, with and without glycosylations ($Gly^{+/-}$).

789

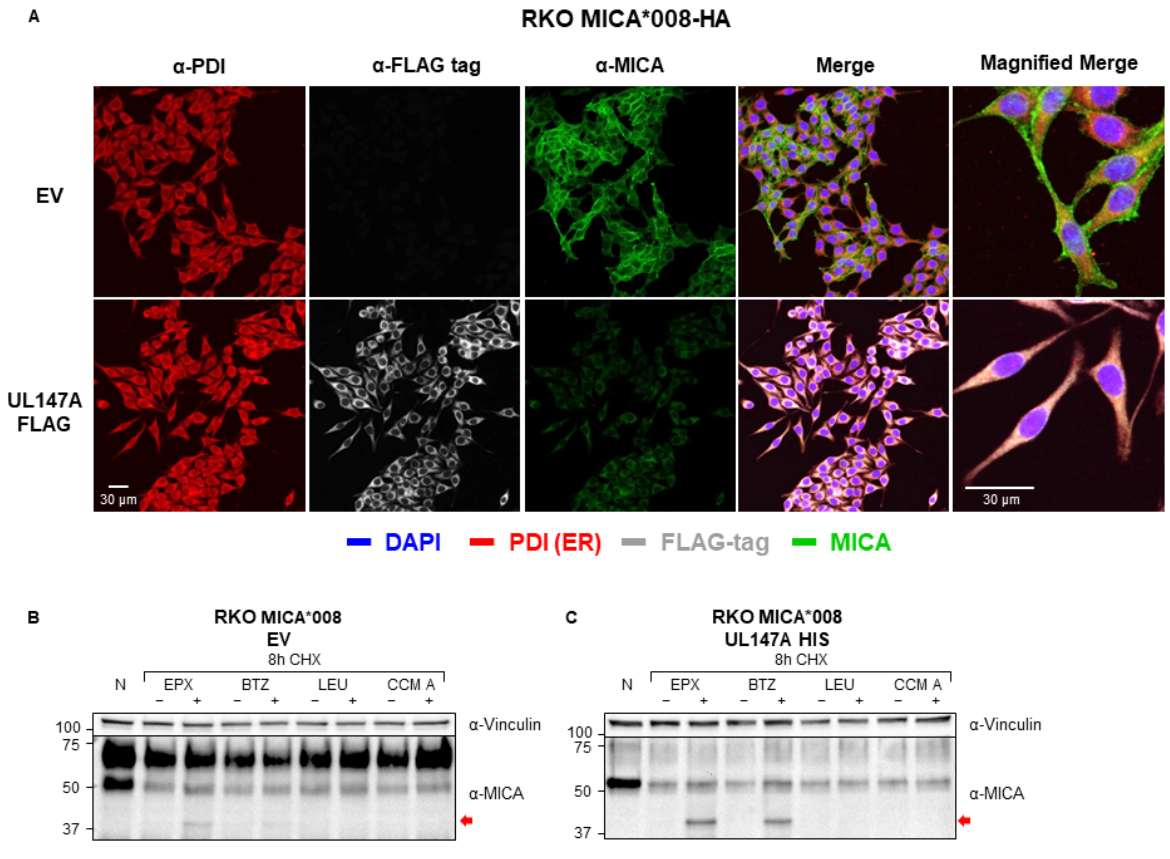

790

791 **Figure 3. UL147A is an ER-resident protein which reduces surface MICA*008 but**

792 **spares ER-resident MICA*008.** (A) RKO MICA*008-HA cells transduced with an EV or

793 with UL147A-FLAG were grown on glass slides, fixed and stained with an anti-protein

794 disulfide isomerase (PDI) antibody (ER marker; red), an anti-FLAG-tag antibody (grey) and

795 an anti-MICA antibody (green). Nuclei were stained with DAPI (blue). Images were captured

796 by confocal microscopy. (B-C) RKO-MICA*008-HA cells expressing an EV (B) or N-

797 terminally tagged UL147A (C) were left untreated (N), or incubated for 8 hours with the

798 translation inhibitor cycloheximide (CHX, 50 μg/ml), in combination with one of two

799 lysosomal inhibitors: leupeptin (LEU, 100 μg/ml) and concanamycin A (CCM A, 20 nM), or

800 with one of two proteasomal inhibitors: epoxomicin (EPX, 8 μM) and bortezomib (BTZ, 8

μM). Each inhibitor was matched with an appropriate mock-treatment (DMSO or DDW). Following treatment, cells were lysed and blotted with anti-MICA. Anti-vinculin served as loading control. Representative of two independent experiments.

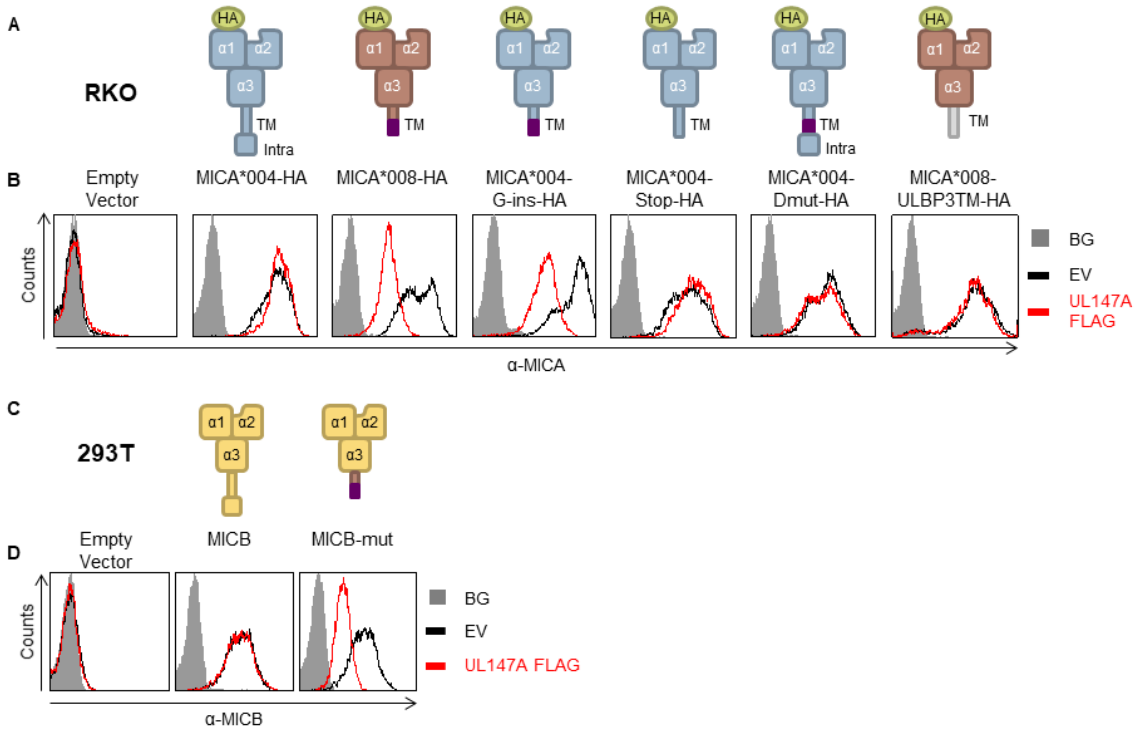

805

806 **Figure 4. Specific MICA*008 features are required for UL147A-mediated**
807 **downregulation.** (A) Schematic representation of the MICA mutants and chimeric proteins
808 used to identify which feature of MICA*008 is recognized by UL147A. Annotated are the N-
809 terminal HA tag, α1-3 domains, the transmembrane (TM) domain and the intracellular tail
810 (intra). The frameshifted MICA*008 sequence is shown in purple. (B) FACS staining of
811 MICA expression in RKO cells transduced with the MICA proteins described in (A) and co-
812 transduced with an EV (black histogram) or with UL147A-FLAG (red histogram). Gray-
813 filled histograms represent secondary antibody staining of EV cells, all control stainings were
814 similar to the one shown. Representative of three independent experiments. (C) Schematic
815 representation of MICB and a mutated MICB with MICA*008's TM domain. (D) Anti-

816 MICB FACS staining of 293T cells transduced with an EV (left histogram); with WT MICB
817 (middle histogram); or with MICB-mut (right) and co-transduced with an EV (black
818 histogram) or with UL147A-FLAG (red histogram). Gray-filled histograms represent
819 secondary antibody staining of EV cells, all control stainings were similar to the one shown.
820 Representative of three independent experiments.

Figure 5

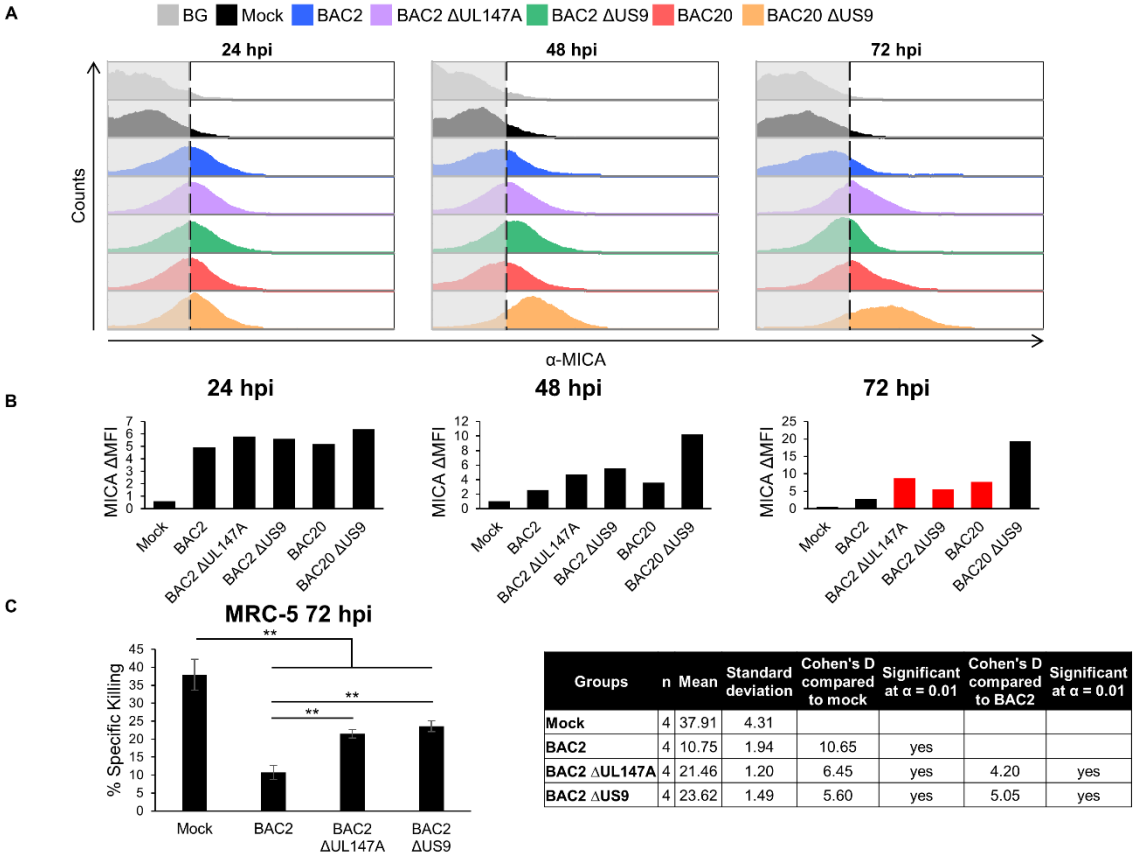

Groups	n	Mean	Standard deviation	Cohen's D compared to mock	Significant at α = 0.01	Cohen's D compared to BAC2	Significant at α = 0.01
Mock	4	37.91	4.31				
BAC2	4	10.75	1.94	10.65	yes		
BAC2 ΔUL147A	4	21.46	1.20	6.45	yes	4.20	yes
BAC2 ΔUS9	4	23.62	1.49	5.60	yes	5.05	yes

Figure 5. UL147A-mediated MICA*008 downregulation leads to reduced NK-mediated killing of HCMV-infected cells. (A-B) MRC-5 HLFs (MICA*008 homozygous) were either mock infected or infected with the indicated HCMV strains. Cells were harvested at the indicated number of hours post infection (hpi). MICA surface expression was assayed by flow cytometry (A) and quantified (B). Grey-filled histograms represent an isotype control staining of mock-infected cells, similar to all other cells. Red bars highlight deletion mutants whose phenotype matches that of UL*b'*-deficient virus. Representative of three independent experiments. (C) MRC-5 HLFs were mock infected or infected with BAC2, BAC2 ΔUL147A or BAC2 ΔUS9. The cells were radioactively labeled overnight and harvested at 72 hpi, and then incubated with NK cells. NK cell mediated killing was then measured by radioactivity

release. Error bars show STDEV for quadruplicates. A one-way ANOVA was performed to evaluate significance. There was a significant effect at the $p<0.05$ level for all conditions [$F(3,2) = 76.8$, $p = 4.22 \cdot 10^{-8}$]. A post-hoc contrast test was used to compare the killing percentage of mock infected cells to that of each infected cell, and to compare BAC2 killing percentage to the two mutants. ** = $p<0.01$. Full statistical values appear in the figure. Representative of two independent experiments from two NK donors.

838

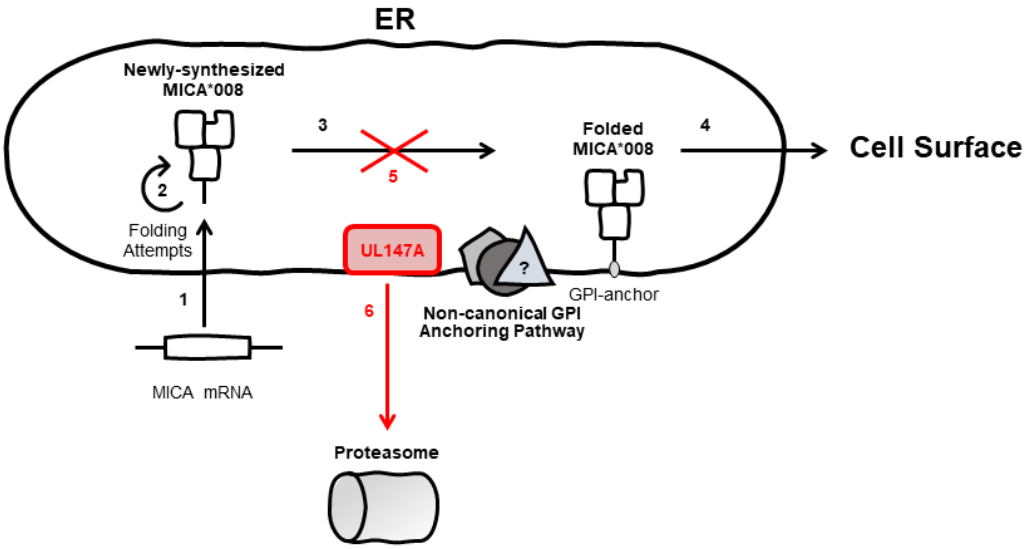

839

840 **Figure 6. UL147A targets GPI-anchored MICA*008 to proteasomal degradation.** A
841 model of UL147A's effect on MICA*008: (1) following HCMV infection, MICA*008
842 mRNA is upregulated and the protein is translated into the ER lumen. (2) The immature, non-
843 anchored form of MICA*008 is retained for repeated folding attempts. (3) MICA*008
844 undergoes GPI anchoring via an unknown non-canonical pathway and (4) subsequently
845 reaches the cell surface. (5) UL147A targets this stage and diverts non-anchored MICA*008
846 to the cytosol, (6) where it is subsequently degraded by the proteasome. Viral mechanisms
847 are marked in red.

848 **Supplemental Material**

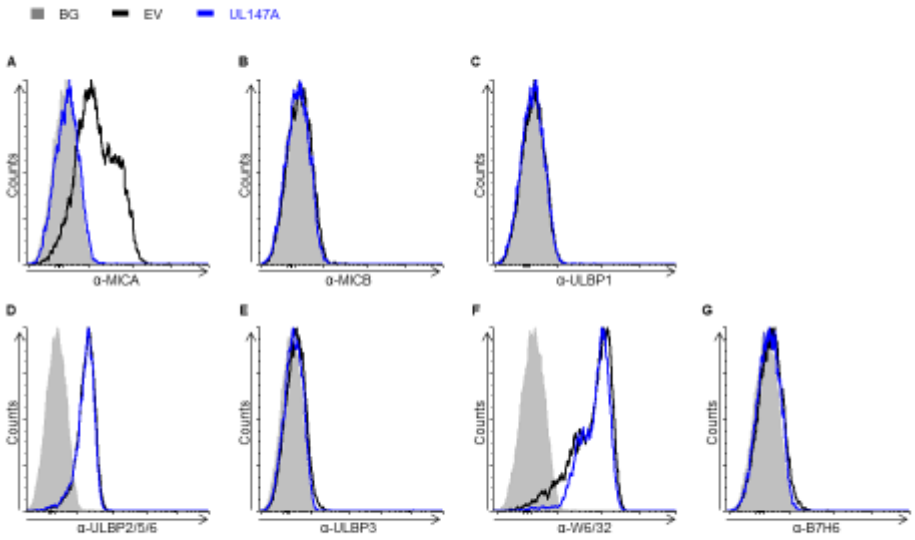

849

850 **Figure S1, associated with figure 2. UL147A specifically targets MICA*008.** FACS
851 staining for NK ligands (indicated in the figure) of RKO MICA*008 cells transduced with an empty
852 vector (EV; black histogram) or UL147A (blue histogram). Gray-filled histograms represent
853 secondary antibody staining. Representative of two independent experiments.

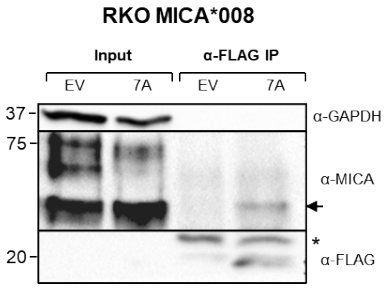

Figure S2, associated with figure 3. UL147A interacts with the ER-resident form of MICA*008. Lysates prepared from RKO MICA*008-HA cells co-transduced with EV or UL147A were immunoprecipitated using anti-FLAG tag antibody. Western blot was performed using anti-FLAG tag and anti-MICA to visualize protein co-precipitation, with anti-GAPDH as input loading control. Arrow indicates a MICA*008 band which specifically co-precipitated with UL147A * - antibody light chain.

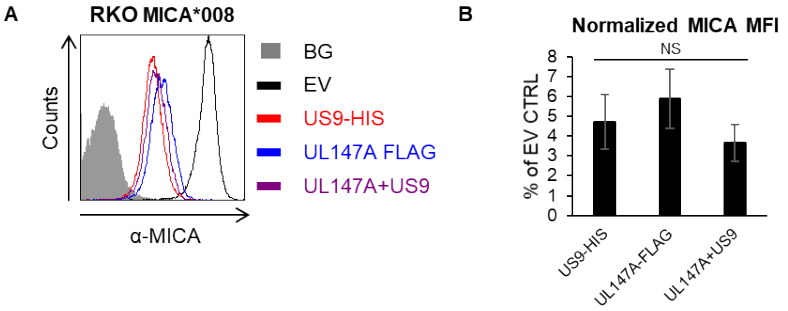

862

863 **Figure S3, associated with figure 5. UL147A and US9 are redundant in an**

864 **overexpression model.** (A) RKO MICA*008-HA cells were transduced with an EV, US9-

865 HIS, UL147A-FLAG or with US9-HIS and UL147A-FLAG together to assess synergism

866 between the two. MICA surface expression was assayed by flow cytometry. Gray-filled

867 histograms represent secondary antibody staining of EV cells, all control stainings were

868 similar to the one shown. Representative of three independent experiments. (B)

869 Quantification of MICA surface expression shown in (A), normalized to the EV control.

870 Error bars show SEM for three independent experiments. A one-way ANOVA was

871 performed to compare the normalized MICA MFIs between US9, UL147A and the two

872 proteins together. There was no significant effect at the $p<0.05$ level for all conditions [F

873 $(2,6) = 0.76$, $p = 0.5$].

874